



1     **Decadal Evolution of Aerosol-Mediated Ozone Responses in Eastern**  
2     **China under Clean Air Actions and Carbon Neutrality Policies**

3     Yasong Li<sup>1,3</sup>, Chen Li<sup>2</sup>, Yaoyu Li<sup>1</sup>, Tijian Wang<sup>3\*</sup>, Mengmeng Li<sup>3</sup>, Yawei Qu<sup>4</sup>, Hao Wu<sup>5</sup>, Min, Xie<sup>6</sup>, Yanjin  
4     Wang<sup>1</sup>

5     1.   *College of Environmental Economics, Henan Finance University, Zhengzhou, 450046, China*

6     2.   *School of Energy and Chemical Engineering, Tianjin Renai College, Tianjin, 301636, China*

7     3.   *School of Atmospheric Sciences, Nanjing University, Nanjing, 210023, China*

8     4.   *College of Intelligent Science and Control Engineering, Jinling Institute of Technology, Nanjing, 211112, China*

9     5.   *Key Laboratory of Transportation Meteorology of China Meteorological Administration, Nanjing Joint Institute for*  
10     *Atmospheric Sciences, Nanjing, China*

11    6.   *School of Environment, Nanjing Normal University, Nanjing 210023, China*

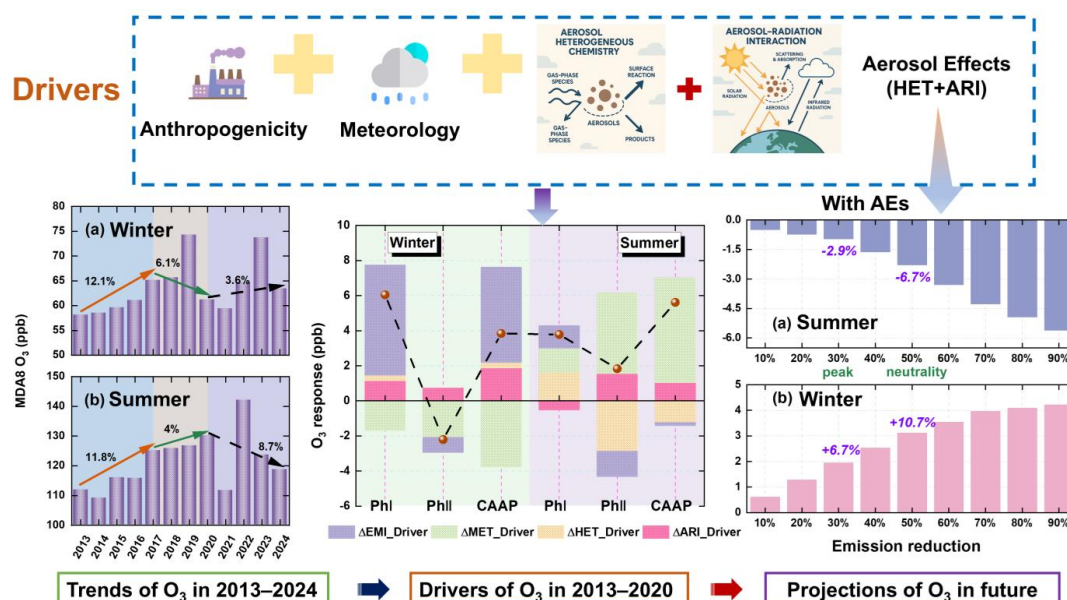
12    **Correspondence to: Tijian Wang (tjwang@nju.edu.cn)**



### Abstract:

Despite substantial reductions in  $\text{PM}_{2.5}$  and other pollutants, ozone ( $\text{O}_3$ ) in eastern China has increased over the past decade, yet the influence of aerosol processes—including aerosol–radiation interactions (ARI) and heterogeneous chemistry (HET)—on these trends remains poorly understood, particularly during Clean Air Action Plan (Phase I: 2013–2017; Phase II: 2018–2020) and under carbon neutrality pathways. We applied a phase- and season-resolved WRF-Chem framework with explicit ARI and HET to quantify historical and projected  $\text{O}_3$  changes in the Yangtze River Delta (YRD), linking aerosol effects with clean air actions and carbon-neutrality pathways. The results revealed that anthropogenic emissions and meteorological variability respectively dominated winter and summer  $\text{O}_3$  increases. Winter  $\text{O}_3$  increases were dominated by ARI: large aerosol reductions enhanced solar radiation, temperature, and photolysis, resulting in a photochemical  $\text{O}_3$  rise (+1.14 (+0.74) ppb in Phase I (II)). Summer  $\text{O}_3$  was more sensitive to HET: initial aerosol decreases weakened radical scavenging, promoting  $\text{O}_3$  formation (+1.62 ppb), whereas the weakening of this effect during Phase II reduced  $\text{O}_3$  (-2.86 ppb). Accounting for aerosol effects (AEs=ARI+HET), reductions in  $\text{PM}_{2.5}$  and  $\text{NO}_x$  increased  $\text{O}_3$ , while VOCs reductions consistently lowered  $\text{O}_3$  in both seasons. Under carbon peaking and neutrality scenarios with AEs, winter  $\text{O}_3$  increased by 6.7% and 10.7%, whereas summer  $\text{O}_3$  decreased by 2.9% and 6.7%, highlighting seasonally contrasting responses. These results underscore the necessity of explicitly accounting for multi-path aerosol– $\text{O}_3$  interactions in both near-term air quality management and long-term climate mitigation to prevent unintended trade-offs and maximize co-benefits.

### Graphical Abstract:





## 32 1. Introduction

33 Over the past decade, China has made remarkable progress in improving air quality, primarily driven by stringent emission  
34 control policies targeting key pollutants such as sulfur dioxide (SO<sub>2</sub>), nitrogen oxides (NO<sub>x</sub>), and fine particulate matter (PM<sub>2.5</sub>).  
35 Landmark initiatives—including the Air Pollution Prevention and Control Action Plan (Phase I: 2013–2017), the Three-Year  
36 Blue Sky Protection Campaign (Phase II: 2018–2020), and the more recent dual-carbon strategy—have led to substantial and  
37 sustained reductions in PM<sub>2.5</sub> across major urban agglomerations (Geng et al., 2024; Zhai et al., 2019). However, in sharp  
38 contrast to these successes, ground-level O<sub>3</sub> have continued to rise, particularly in economically developed regions such as  
39 Beijing–Tianjin–Hebei (BTH, (Zhao et al., 2023; Dai et al., 2023)), the Yangtze River Delta (YRD, (Li et al., 2023; Hu et al.,  
40 2025)), and the Pearl River Delta (PRD, (Chen et al., 2020)). For example, Yan et al. (2024) reported that the annual mean  
41 maximum daily 8-hour average (MDA8) O<sub>3</sub> in major Chinese cities increased from 106.0 µg m<sup>-3</sup> in 2013 to 131.1 µg m<sup>-3</sup> in  
42 2022, with the most pronounced growth observed in the BTH and YRD regions. The emerging decoupling between PM<sub>2.5</sub> and  
43 O<sub>3</sub> trends underscores the growing complexity of air pollution control in China, suggesting that conventional precursor-  
44 oriented mitigation strategies may be insufficient to address secondary pollutants formed through nonlinear atmospheric  
45 processes. The increasing frequency and intensity of O<sub>3</sub> pollution episodes not only pose serious risks to human health and  
46 ecosystems (Liu et al., 2018; Li et al., 2020) but also diminish the co-benefits of PM<sub>2.5</sub> mitigation. As China advances toward  
47 its dual goals of high-quality development and carbon neutrality, elucidating the mechanisms behind this counterintuitive O<sub>3</sub>  
48 rise has become both a scientific imperative and a policy priority.

49 Extensive research has identified anthropogenic emissions and meteorological variability as the two dominant drivers of  
50 observed O<sub>3</sub> increases (Ma et al., 2023; Sun et al., 2019; Shao et al., 2024; Ni et al., 2024), particularly during the early stages  
51 of the Clean Air Action Plan (CAAP). For instance, Dang et al. (2021) used the GEOS-Chem model to show that during the  
52 summer of 2012–2017, meteorological changes accounted for 49% of the O<sub>3</sub> increase in the BTH region and 84% in the YRD,  
53 while emission changes explained 39% and 13%, respectively. Recent efforts combining numerical modeling with machine  
54 learning have further highlighted the critical roles of solar radiation and temperature, especially during the COVID-19  
55 lockdown. Zhang et al. (2025) attributed approximately 94% of the summer O<sub>3</sub> increase in the Hangzhou Bay area from 2019  
56 to 2022 to meteorological influences, noting a growing dominance of meteorological drivers over emission-related factors. In  
57 addition, innovative metrics such as the O<sub>3</sub>-specific emission–meteorology index (EMI/O<sub>3</sub>) have been proposed to quantify  
58 these contributions, revealing that summer O<sub>3</sub> increases in cities like Beijing and Shanghai were largely governed by volatile  
59 organic compound (VOCs) emissions and meteorological shifts (Lu et al., 2025).

60 Beyond emissions and meteorology, aerosol effects (AEs) have emerged as important, though often overlooked, regulators  
61 of surface O<sub>3</sub>. Aerosols influence O<sub>3</sub> formation through two principal mechanisms: aerosol–radiation interaction (ARI), which



alter photolysis rates and boundary layer dynamics, and heterogeneous chemistry (HET), which removes hydroperoxyl ( $\text{HO}_2$ ) radical and suppresses  $\text{O}_3$  formation (Li et al., 2025; Li et al., 2024b; Li et al., 2019a; Gao et al., 2018). As aerosol loading has substantially declined under clean air policies, the magnitudes and directions of these mechanisms may have shifted. For instance, Yu et al. (2019) found that reductions in  $\text{PM}_{2.5}$  contributed to approximately 22% of the observed  $\text{O}_3$  increase in the YRD during 2013–2017. Yang et al. (2024) quantified a 0.81 ppb increase in summer  $\text{O}_3$  linked to the weakening of ARI under lower aerosol conditions. Our previous research demonstrated that the reduced aerosol suppression of photochemistry via ARI, photolysis inhibition, and HET collectively amplified  $\text{O}_3$  increases by 22.2%–57.3% between 2014 and 2020 (Li et al., 2024a). Similarly, Liu et al. (2023) identified weakened HET as the dominant mechanism behind  $\text{O}_3$  increases across both phases of the CAAP. Moreover, precursor– $\text{O}_3$  relationships are strongly modulated by background aerosol levels, further emphasizing the need to assess  $\text{O}_3$  responses under evolving aerosol conditions to ensure the effectiveness of co-control strategies.

Despite increasing recognition of the role of aerosols in modulating surface  $\text{O}_3$ , several critical knowledge gaps remain. Most existing studies tend to isolate either ARI or HET rather than evaluate their combined and potentially synergistic effects. Additionally, few investigations adopt a phase- and season-resolved framework aligned with policy implementation timelines, and even fewer consider long-term projections under carbon neutrality pathways. Furthermore, the spatial heterogeneity and nonlinear chemical responses of  $\text{O}_3$  under dynamic aerosol environments remain poorly characterized, particularly in densely populated and industrialized regions like the YRD. To address these gaps, this study employs an improved WRF-Chem modeling framework to conduct a comprehensive, phase-, season-, and mechanism-resolved assessment of AEs in the YRD from 2013 to 2024. By explicitly disentangling the effects of ARI and HET and integrating them with historical emission changes, meteorological variability, and future carbon neutrality-driven mitigation scenarios, we aim to systematically quantify the drivers of past  $\text{O}_3$  trends and predict their future trajectories. Furthermore, we evaluate the seasonal and spatial  $\text{O}_3$  responses to the reduction of individual precursors ( $\text{PM}_{2.5}$ ,  $\text{NO}_x$ , VOCs,  $\text{NH}_3$ , and  $\text{SO}_2$ ), offering mechanistic insights into when and where synergistic air quality–climate benefits can be effectively achieved. These findings provide a scientific foundation for designing regionally tailored and seasonally adaptive  $\text{O}_3$  control strategies aligned with China’s dual goals of pollution reduction and carbon neutrality.

## 2. Methodology

### 2.1 Model and dataset

This study employed an enhanced version of the Weather Research and Forecasting model coupled with Chemistry (WRF-Chem, version 3.7.1, (Grell et al., 2005)) to investigate the drivers of surface  $\text{O}_3$  variability over eastern China during two key phases of the CAAP (Phase I and Phase II). In addition to examining the roles of anthropogenic emission changes and meteorological variability, particular emphasis was placed on quantifying the impacts of two critical aerosol-related processes



(ARI and HET) on long-term O<sub>3</sub> trends. Furthermore, we explored the O<sub>3</sub> responses to precursor emission reductions and assessed the implications of future carbon neutrality-driven emission scenarios on surface O<sub>3</sub> under the influence of AEs (ARI+HET). As an extension of our previous modeling work, the WRF-Chem configuration followed the setup established in earlier studies (Li et al., 2024a; Li et al., 2024b). A three-level nested domain structure was adopted, covering East Asia (outer domain), eastern China (middle domain), and the YRD (innermost domain), as illustrated in Figure S1. Meteorological initial and boundary conditions were obtained from the National Centers for Environmental Prediction Final (NCEP FNL) reanalysis data, with a horizontal resolution of 1° × 1°. Anthropogenic emissions were derived from the Multi-resolution Emission Inventory for China (MEIC v1.4), developed by Tsinghua University, which provides gridded emissions of major air pollutants at a resolution of 0.25° × 0.25°. Biogenic emissions were generated online using the Model of Emissions of Gases and Aerosols from Nature (Guenther et al., 2006).

Model simulations were conducted for January and July to represent typical winter and summer conditions, respectively. The simulation periods extended from December 29 to February 1 for winter and from June 28 to August 1 for summer, with the first three days discarded as spin-up for chemical initialization. In addition to seasonal simulations, we evaluated the decadal evolution of MDA8 O<sub>3</sub> in the YRD from 2013 to 2024 for both seasons. Observed hourly surface O<sub>3</sub> data were obtained from China's national air quality monitoring network, maintained by the Ministry of Ecology and Environment (MEE). The spatial distribution and technical specifications of the monitoring sites are detailed in our previous publications.

## 2.2 Aerosol effects enhancement

This study systematically assessed the impacts of aerosol-related processes on O<sub>3</sub> variability in the context of China's historical CAAP and future carbon neutrality targets. Two key mechanisms (ARI and HET) were incorporated into the WRF-Chem framework to capture the coupled physical and chemical influences of aerosols on O<sub>3</sub> formation. The implementation and validation of these modules were based on our previous studies and are briefly summarized here (Li et al., 2024b). The ARI mechanism affects O<sub>3</sub> primarily through two pathways: (1) modifying photolysis rates via aerosol extinction, and (2) altering meteorological fields through aerosol–radiation feedback (ARF). Although the default WRF-Chem framework includes ARF, the embedded Fast-J photolysis scheme lacks a dynamic linkage to aerosol optical properties, thereby omitting the direct impact of aerosol extinction on photolysis. To address this limitation, we developed a customized interface that dynamically couple aerosol optical parameters (e.g., scattering and absorption coefficients) with the Fast-J module. This enhancement enabled accurate calculation of aerosol optical depth and allowed photolysis rates to respond realistically to spatiotemporal aerosol variability.

The HET mechanism was implemented within the Model for Simulating Aerosol Interactions and Chemistry (MOSAIC) aerosol module to simulate heterogeneous reactions involving O<sub>3</sub>, NO<sub>x</sub>, and hydrogen on aerosol surfaces. This module accounted for multiphase uptake processes, enhancing the model's ability to capture the complex interplay between aerosols



and oxidants and to represent secondary chemical transformations. Both ARI and HET mechanisms were consistently applied in all historical and scenario-based simulations conducted in this study, ensuring internally consistent representation of aerosol–O<sub>3</sub> interactions. Key parameters—such as uptake coefficients, aerosol surface area densities, and photolysis scaling factors—followed values validated in our previous modeling work (Li et al., 2024b). The improved WRF-Chem system has been extensively evaluated and shown to reliably reproduce meteorological conditions, aerosol properties, and trace gas concentrations over China, particularly in the YRD region (Qu et al., 2023; Li et al., 2018).

### 2.3 Numerical experimental designs

To systematically assess the respective and combined impacts of anthropogenic emission changes, meteorological variability, and aerosol-related mechanisms on O<sub>3</sub>, we designed three sets of numerical experiments using the enhanced WRF-Chem modeling framework (Table 1). These experiments focused on: (1) historical attribution, (2) precursor-specific sensitivity, and (3) future multi-pollutant mitigation pathways.

#### 1) SET1: Historical Attribution Simulations (2013–2020).

This set aimed to quantify the primary drivers of O<sub>3</sub> variations during two critical phases of CAAP (Phase I and Phase II). A total of 11 simulations were conducted, addressing emission changes, meteorological effects, and aerosol mechanisms:

**Emission-driven effects:** To isolate the influence of anthropogenic emission changes, three simulations were performed under fixed meteorological conditions (2020) with AEs turned off (13E20M\_NOALL, 17E20M\_NOALL, 20E20M\_NOALL). The differences among these runs quantify the net O<sub>3</sub> response to evolving emissions alone.

**Meteorology-driven effects:** To evaluate the role of meteorological variability, three additional simulations used fixed emissions (2013) and excluded AEs (13E13M\_NOALL, 13E17M\_NOALL, 13E20M\_NOALL). Differences among these runs reflect the contribution of meteorological factors to O<sub>3</sub> trends.

**Aerosol effects (AEs):** For each emission year (2013, 2017, and 2020), three parallel simulations were conducted: (i) with all aerosol-related processes enabled (AEs), (ii) with heterogeneous chemistry disabled (NOHET), and (iii) with all aerosol effects turned off (NOALL). By comparing pairs of these simulations (e.g., AEs–NOHET, NOHET–NOALL, AEs–NOALL), we quantified the isolated contributions of HET, ARI, and their combined impacts. For example, the difference between 20E20M\_AEs and 20E20M\_NOHET isolated the HET contribution under 2020 emission conditions, while 20E20M\_NOHET versus 20E20M\_NOALL captured the ARI effect. This approach was applied to all emission years to evaluate the phase-resolved impacts of aerosol-related mechanisms on O<sub>3</sub> trends. Schematic diagram of scenario design and ozone responses to aerosol-related processes in different emission phases were shown in Figure 1.

#### 2) SET2: Single-Precursor Sensitivity Experiments (2020 baseline).

To investigate the nonlinear O<sub>3</sub> responses to individual precursor controls under active aerosol conditions, we conducted sensitivity experiments based on the 2020 emissions inventory. Each experiment involved a 25% and 50% reduction in one of



154 five key precursors—primary  $\text{PM}_{2.5}$ ,  $\text{NO}_x$ , VOCs,  $\text{SO}_2$ , and  $\text{NH}_3$ —while holding other emissions constant. Reductions in  
155 primary  $\text{PM}_{2.5}$  included both black carbon (BC) and organic carbon (OC). All simulations retained both HET and ARI  
156 mechanisms to ensure consistent physical and chemical representations of AEs.

157 3) SET3: Multi-Pollutant Co-Reduction Experiments (Future Scenarios).

158 To explore the effects of future mitigation strategies aligned with China's dual-carbon goals (carbon peaking and carbon  
159 neutrality), a series of simulations were conducted with coordinated reductions in all anthropogenic emissions. We referred to  
160 the mid- and long-term projections evaluated by Cheng et al. (2021), who analyzed China's air quality improvement trajectory  
161 under the dual-carbon strategy. Their study estimated that by 2030, total anthropogenic pollutant emissions would decrease by  
162 26%–32% relative to 2020 levels. However, after 2030, the mitigation pace is projected to slow, with a maximum reduction of  
163 approximately 31% by 2060 compared to 2030 levels. Guided by these projections, we selected two representative emission  
164 reduction levels—30% and 50%—to approximate China's carbon peaking (2030) and carbon neutrality (2060) targets, respectively.  
165 To further investigate the nonlinear nature of  $\text{O}_3$  responses under deeper mitigation, additional reduction scenarios of 10%,  
166 20%, 40%, 60%, 70%, 80%, and 90% were included. In all scenarios, emissions of primary  $\text{PM}_{2.5}$ ,  $\text{NO}_x$ , VOCs,  $\text{SO}_2$ , and  $\text{NH}_3$   
167 were proportionally reduced, representing a co-control strategy for multiple pollutants. Aerosol-related processes were kept  
168 active across all future simulations to ensure realism in atmospheric feedbacks.

169 All experiments (SET1, SET2, SET3) were conducted for the months of January and July, representing winter and summer  
170 conditions, respectively, to capture seasonal contrasts in  $\text{O}_3$  formation. Daily mean  $\text{O}_3$  concentrations were used as the primary  
171 diagnostic metric. Although ARI primarily influence daytime photochemistry through modified photolysis and boundary layer  
172 dynamics, heterogeneous chemistry played a crucial role in nighttime radical removal and  $\text{O}_3$  loss. Therefore, the commonly  
173 used MDA8  $\text{O}_3$  may underestimate full-day aerosol effects. Using daily mean  $\text{O}_3$  provided a more integrated and representative  
174 metric to capture the combined impacts of aerosol interactions over a 24-hour period.



175

**Table 1** Summary of scenario configurations for numerical simulations.

Scenario sets	Scenario ID	Anthropogenic emissions	Meteorology	HET <sup>a</sup>	ARI <sup>b</sup>	Purpose
SET1	20E20M_AEs	2020	2020	✓	✓	Baseline scenario with full aerosol effects
	20E20M_NOHET			×	✓	Isolate impact of HET
	20E20M_NOALL			×	×	No aerosol effects
	17E20M_AEs	2017		✓	✓	Emission-driven impact (2017 emissions with fixed meteorology)
	17E20M_NOHET			×	✓	Same as above, excluding HET
	17E20M_NOALL			×	×	Same as above, excluding all aerosol effects
	13E20M_AEs	2013		✓	✓	Emission-driven impact (2013 emissions with fixed meteorology)
	13E20M_NOHET			×	✓	Same as above, excluding HET
	13E20M_NOALL			×	×	Same as above, excluding all aerosol effects
	13E13M_NOALL	2013	2013	×	×	Meteorology-driven impact (2013 meteorology with fixed emissions)
	13E17M_NOALL	2013	2017	×	×	Meteorology-driven impact (2017 meteorology with fixed emissions)
SET2	CUT_PM2.5_25/50	25 (50) % reduction in PM <sub>2.5</sub> in 2020	2020	✓	✓	O <sub>3</sub> response to PM <sub>2.5</sub> -only reduction
	CUT_NOx_25/50	25 (50) % reduction in NO <sub>x</sub> in 2020				O <sub>3</sub> response to NO <sub>x</sub> -only reduction
	CUT_VOCs_25/50	25 (50) % reduction in VOCs in 2020				O <sub>3</sub> response to VOCs-only reduction
	CUT_NH <sub>3</sub> _25/50	25 (50) % reduction in NH <sub>3</sub> in 2020				O <sub>3</sub> response to NH <sub>3</sub> -only reduction
	CUT_SO <sub>2</sub> _25/50	25 (50) % reduction in SO <sub>2</sub> in 2020				O <sub>3</sub> response to SO <sub>2</sub> -only reduction
SET3	CUT_MEIC_10	10% reduction in 2020	2020	✓	✓	Representative carbon peak scenario (aligned with 2030 goal)
	CUT_MEIC_20	20% reduction in 2020				
	CUT_MEIC_30	30% reduction in 2020				
	CUT_MEIC_40	10% reduction in 2020				Representative carbon neutrality scenario (aligned with 2060 goal)
	CUT_MEIC_50	50% reduction in 2020				
	CUT_MEIC_60	10% reduction in 2020				
	CUT_MEIC_70	70% reduction in 2020				
	CUT_MEIC_80	10% reduction in 2020				
CUT_MEIC_90	90% reduction in 2020					

176 HET<sup>a</sup>: Heterogeneous chemistry (HET) was enabled when the heterogeneous reaction switch was set to 1, respectively.

177 ARI<sup>b</sup>: Aerosol–radiation interaction (ARI) was considered active when both aer\_ra\_feedback = 1 and aerosol optical properties

178 were transmitted to the photolysis module.





### O<sub>3</sub> responses to aerosol effects in different emission phases

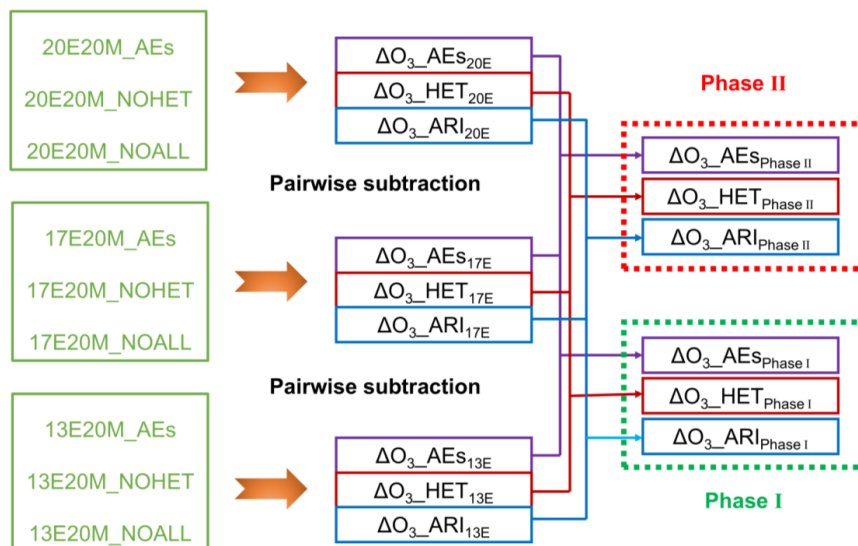


**Figure 1** Schematic diagram of scenario design and ozone responses to aerosol-related processes during the Clean Air Action phases. Note: HET=heterogeneous chemistry, ARI=aerosol-radiation interaction, AEs=aerosol effects (HET+ARI). Scenario IDs such as “13E20M” refer to emission year 2013 with 2020 meteorology.

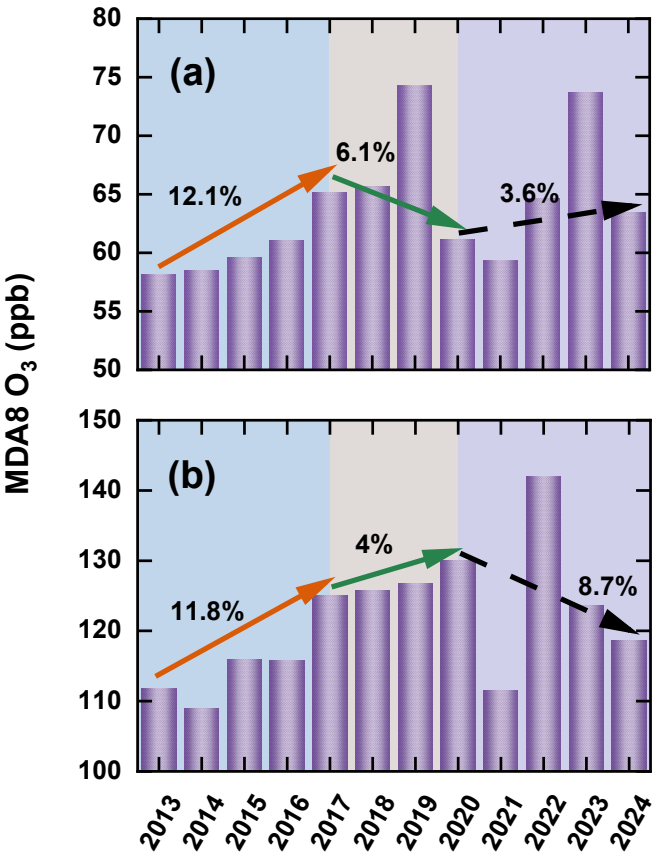
### 2.4 Historical changes in emissions and observed O<sub>3</sub>

Since 2013, the Chinese government had implemented a series of stringent air quality control policies under the CAAP, which led to profound shifts in anthropogenic emissions of key air pollutants. Figure S2 showed the temporal evolution of six major pollutants (SO<sub>2</sub>, primary PM<sub>2.5</sub>, BC, OC, NO<sub>x</sub>, and VOCs) across provinces in YRD from 2013 to 2020. Substantial reductions were observed for all pollutants except VOCs, with SO<sub>2</sub>, primary PM<sub>2.5</sub>, BC, OC and NO<sub>x</sub> decreasing by 69.7%, 46.9%, 40.4%, 38.0%, and 27.9%, respectively. During Phase I, emission control efforts had primarily targeted reductions in PM<sub>2.5</sub>. This focus resulted in significant decreases in primary particulate emissions: primary PM<sub>2.5</sub>, BC, and OC were reduced by 37.0%, 30.0%, and 27.3%, respectively. Simultaneously, key precursors such as SO<sub>2</sub> and NO<sub>x</sub> declined by 56.4% and 19.8%. However, due to the lack of targeted VOCs control measures during this period, VOCs emissions increased by 7.1%, largely driven by industrial processes and solvent usage (Li et al., 2019b). Phase II marked a strategic shift toward more balanced control of NO<sub>x</sub> and VOCs. While emissions of SO<sub>2</sub>, NO<sub>x</sub>, and particulate matter continued to decrease, the rate of reduction slowed compared to Phase I. Specifically, NO<sub>x</sub> and VOCs emissions decreased by only 7.4% and 4.6%, respectively. Overall, VOCs emissions in the YRD still showed a net increase of 2.2% over the full 2013–2020 period. Spatially, the most pronounced emission reductions occurred in the northwestern and central YRD subregions (Figure S3), consistent with national trends and findings from earlier studies (Liu et al., 2023; Yan et al., 2024).

In addition to modifying emissions, the CAAP brought about substantial changes in observed O<sub>3</sub>. Figure 2 illustrated the annual variation of the MDA8 O<sub>3</sub> in winter and summer across the YRD based on ground-based observations from 2013 to



200 2024. In winter, O<sub>3</sub> increased by approximately 7 μg m<sup>-3</sup> during 2013–2017, at an average annual growth rate of 3%. This trend  
201 reversed during 2017–2020, with a decrease of 4 μg m<sup>-3</sup> (2% per year), followed by a modest increase of 2.2 μg m<sup>-3</sup> (0.91%  
202 per year) between 2020 and 2024. In summer, O<sub>3</sub> rose by 13.2 μg m<sup>-3</sup> during 2013–2017, continued to increase by 4.9 μg m<sup>-3</sup>  
203 from 2017 to 2020, and then declined sharply by 11.4 μg m<sup>-3</sup> during 2020–2024. These results suggested that in the early phase  
204 of clean air efforts, the insufficient control of O<sub>3</sub> precursors contributed to significant increases in both winter and summer O<sub>3</sub>.  
205 However, stronger VOCs and NO<sub>x</sub> control measures in recent years appeared to mitigate this upward trend. A particularly  
206 sharp drop in O<sub>3</sub> between 2020 and 2021 was likely caused by a combination of intensified emission reductions and unusual  
207 meteorological conditions (Yin et al., 2021). Overall, observed MDA8 O<sub>3</sub> in the YRD increased by 12.1% in winter and 11.8%  
208 in summer during 2013–2017. In the subsequent periods (2017–2020 and 2020–2024), winter O<sub>3</sub> levels first declined and then  
209 rebounded, while summer O<sub>3</sub> initially rose and then decreased. The underlying causes of these contrasting patterns were  
210 explored in detail in the Results section. Note that this study did not focus on the spatial distribution of O<sub>3</sub> changes, as this  
211 topic has already been extensively examined in previous literature (Hu et al., 2025; Zhao et al., 2023).



212  
213 **Figure 2** Annual trends in winter (a) and summer (b) MDA8 O<sub>3</sub> concentrations (ppb) over the Yangtze River Delta (YRD)  
214 from 2013 to 2024 based on continuous ground-based observations.



### 215 3. Results and discussion

216 Before presenting the simulation outcomes, it is important to clarify that the performance of the enhanced WRF-Chem  
217 model, particularly its representation of meteorological fields, and air pollutant concentrations. The 20E20M\_AEs scenario,  
218 which incorporates 2020 anthropogenic emissions and meteorological conditions with both ARI and HET effects activated,  
219 was deemed the most realistic representation of the atmospheric state during that year. The accuracy of simulated  
220 meteorological parameters and pollutant concentrations under this scenario has been thoroughly validated against ground-  
221 based observations in earlier work and is therefore not reiterated here (Li et al., 2024a). Accordingly, the subsequent sections  
222 focus on interpreting the key drivers, underlying mechanisms, and broader implications of modeled O<sub>3</sub> changes under various  
223 historical and future emission scenarios, with a particular emphasis on the role of aerosol-related processes.

#### 224 3.1 Attribution of historical seasonal O<sub>3</sub> changes to emissions and meteorology

225 We conducted a series of attribution simulations (SET1) to elucidate the dominant drivers of O<sub>3</sub> variability in YRD over  
226 the past decade. To isolate the effects of emission changes, we excluded aerosol interactions (i.e., the NOALL cases) and held  
227 meteorological conditions constant at 2020 levels while varying the emission year. The resulting O<sub>3</sub> responses are presented  
228 in Figure 3. During Phase I, emission reductions unexpectedly led to O<sub>3</sub> increases of 6.3 ppb in winter and 1.3 ppb in summer.  
229 In contrast, Phase II witnessed coordinated NO<sub>x</sub> and VOCs controls, leading to O<sub>3</sub> reductions of 0.9 ppb (winter) and 1.5 ppb  
230 (summer). These contrasting outcomes reflect the nonlinear chemistry of O<sub>3</sub> formation. While Phase I focused primarily on  
231 reducing PM<sub>2.5</sub> and SO<sub>2</sub>, VOCs emissions remained poorly regulated and even increased, enhancing photochemical activity.  
232 In contrast, Phase II adopted a more balanced control strategy targeting both NO<sub>x</sub> and VOCs, which proved more effective in  
233 mitigating O<sub>3</sub> pollution. Spatially, the strongest O<sub>3</sub> responses occurred in the northwestern and central parts of the YRD,  
234 aligning with regions that experienced the largest emission reductions.

235 To assess the influence of meteorological conditions, we fixed anthropogenic emissions at 2013 levels and varied the  
236 meteorological fields across years. Results revealed seasonally asymmetric impacts: meteorology contributed to wintertime  
237 O<sub>3</sub> declines (1.7 ppb and 2.1 ppb during Phases I and II, respectively), but promoted summertime O<sub>3</sub> increases (1.4 ppb and  
238 4.6 ppb). This highlighted a distinct seasonal asymmetry in meteorological influences on O<sub>3</sub>. As summarized in Table S1,  
239 changes in five key meteorological parameters (shortwave radiation (SW), temperature (T<sub>2</sub>), relative humidity (RH<sub>2</sub>), planetary  
240 boundary layer height (PBLH), and wind speed (WS<sub>10</sub>)) collectively explain these trends. In winter, lower radiation and T<sub>2</sub>,  
241 higher RH<sub>2</sub>, and stronger WS<sub>10</sub> suppressed O<sub>3</sub> formation and accumulation. Conversely, summer conditions characterized by  
242 higher radiation and T<sub>2</sub>, coupled with lower RH<sub>2</sub> and weaker WS<sub>10</sub>, favored O<sub>3</sub> build-up. Although this study does not explicitly  
243 quantify the relative contributions of individual meteorological factors, prior studies (Liu et al., 2023; Yan et al., 2024; Dai et  
244 al., 2024) using multiple linear regression consistently identify SW and T<sub>2</sub> as dominant drivers. Figure S4 presented the spatial  
245 distributions of meteorological changes from 2013 to 2020, revealing that the most pronounced shifts—especially in radiation



246 and temperature-occurred in the central YRD and were more significant in summer, consistent with stronger O<sub>3</sub> responses.

247 In summary, anthropogenic emission changes were the dominant drivers of winter O<sub>3</sub> increases during Phase I. These

248 findings are consistent with earlier research (Cao et al., 2022; Wu et al., 2022), which similarly highlighted that early-phase

249 air quality interventions-though effective in reducing PM<sub>2.5</sub>-often overlooked the complex chemistry of O<sub>3</sub>, particularly the

250 roles of VOCs and NO<sub>x</sub>, thereby unintentionally intensifying O<sub>3</sub> pollution. The transition to coordinated multi-pollutant control

251 strategies in Phase II enabled more effective O<sub>3</sub> mitigation. In addition, the role of meteorology was non-negligible. Our

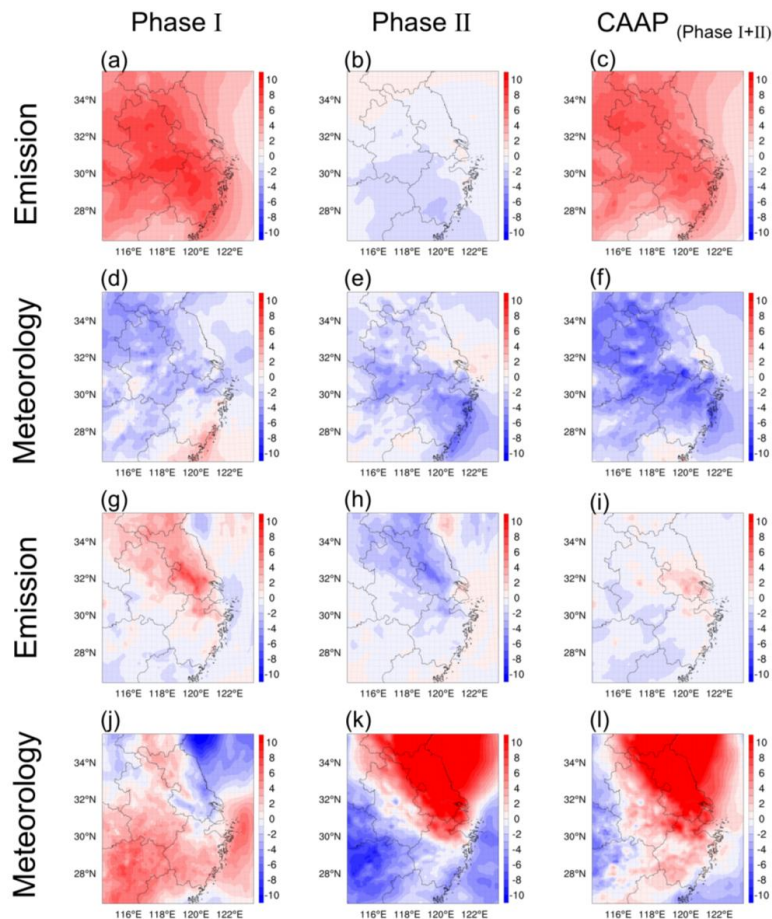
252 findings, in line with those of Liu and Wang (2020), emphasize a pronounced seasonal asymmetry-meteorology suppressed

253 winter O<sub>3</sub> but enhanced summer levels. Notably, wintertime O<sub>3</sub> variability was primarily emission-driven during Phase I, but

254 increasingly influenced by meteorology in Phase II. In contrast, summer O<sub>3</sub> changes were consistently dominated by

255 meteorological variability across both phases. These insights underscore the need for future O<sub>3</sub> control strategies to account

256 for both emissions and meteorological variability, particularly in the context of climate change and evolving pollution regimes.



257  
258 **Figure 3** Seasonal changes in O<sub>3</sub> (ppb) over YRD attributed to anthropogenic emission reductions (b) and meteorological  
259 variability (c) during the two phases of the Clean Air Action Plan. Results are shown for winter (top two rows) and summer  
260 (bottom two rows).



### 261 3.2 Aerosol multi-effects contributions to past seasonal O<sub>3</sub> variations

262 The multifaceted roles of aerosols in regulating O<sub>3</sub>—through aerosol–radiation feedbacks, photolysis attenuation,  
263 and heterogeneous chemistry—have been extensively examined in our previous study (Li et al., 2024b). In this section,  
264 we quantify the seasonal and phase-resolved contributions of two key mechanisms to O<sub>3</sub> changes: ARI and HET, across  
265 the two implementation stages of the CAAP. Detailed descriptions of the experimental configurations are provided in  
266 Section 2.3 and illustrated in Figure 1. Figure 4 displayed the spatial distributions of O<sub>3</sub> responses to ARI and HET  
267 during winter for both CAAP phases over YRD. In Phase I, ARI induced a significant O<sub>3</sub> increase of up to 1.14 ppb  
268 across the region, while the contribution from HET was notably smaller at 0.32 ppb. This indicated that early aerosol  
269 reductions primarily enhanced O<sub>3</sub> via increased solar radiation and associated meteorological feedbacks, rather than  
270 through the suppression of radical uptake on particle surfaces. This finding contrasted with those of Li et al. (2019a),  
271 who—using GEOS-Chem simulations—attributed O<sub>3</sub> increases over the BTH to reduced HO<sub>2</sub> uptake under declining  
272 PM<sub>2.5</sub>. The discrepancy may stem from differences in model representation; our framework explicitly incorporates both  
273 ARI-driven meteorological feedbacks and the direct photolysis attenuation by aerosols, enabling a more comprehensive  
274 simulation of aerosol–radiation interaction. During Phase II, the ARI-induced O<sub>3</sub> increase weakened to +0.74 ppb, and  
275 the contribution from HET became negligible or slightly negative (−0.01 ppb). This suggested that ARI remained the  
276 dominant aerosol-related driver of winter O<sub>3</sub> variability, while the influence of HET diminished. The reduced overall  
277 aerosol impact during this phase was consistent with smaller primary PM<sub>2.5</sub> emission reductions (−8% in Phase II  
278 compared to −37% in Phase I). Summing the contributions from both mechanisms, the total aerosol-driven O<sub>3</sub>  
279 enhancement reached +1.46 ppb in Phase I and +0.73 ppb in Phase II, culminating in a net wintertime increase of +2.2  
280 ppb over the CAAP period.

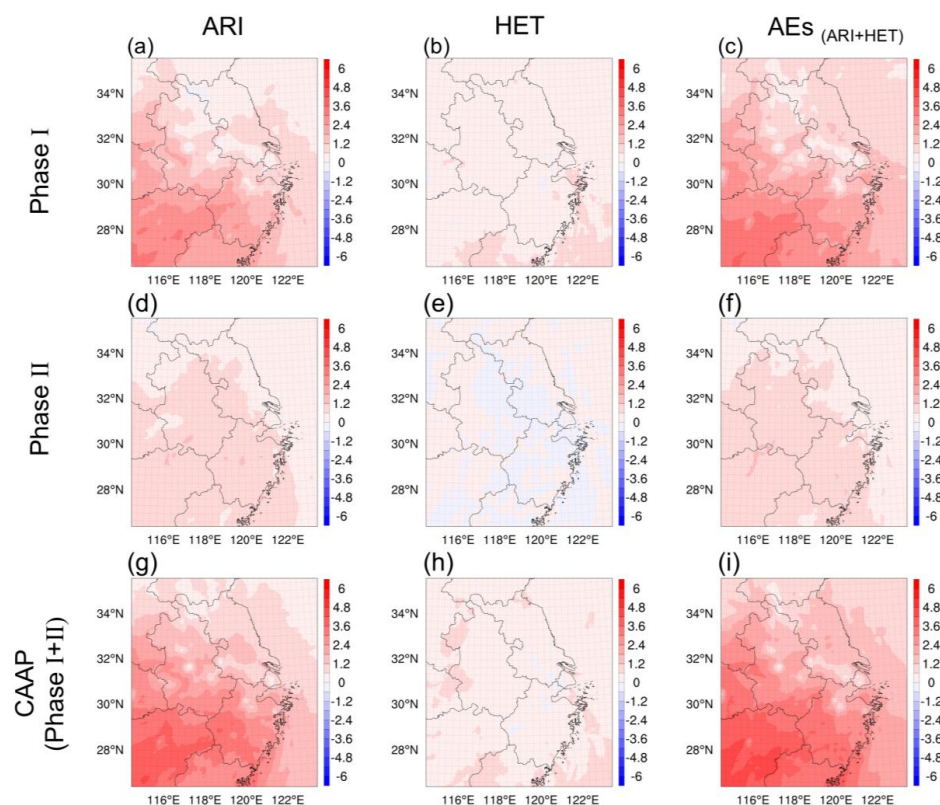


**Figure 4** Spatial distribution of winter  $O_3$  changes (ppb) over the Yangtze River Delta induced by aerosol–radiation interactions (ARI, a, d, g), heterogeneous chemistry (HET, b, e, h) and their combined effects (AEs, c, f, i) during two stages of the Clean Air Action Plan. All results are based on SET1 simulations.

In contrast to winter, summertime  $O_3$  responses to AEs revealed different dominant mechanisms and magnitudes, as shown in Figure 5. In Phase I, HET played a more substantial role, contributing a 1.62 ppb increase, whereas ARI slightly suppressed  $O_3$  by 0.51 ppb. This pattern indicated that under high photochemical activity, reduced particulate matter significantly weakened radical scavenging, thereby elevating  $HO_2$  levels and promoting  $O_3$  formation. During Phase II, however, HET unexpectedly contributed a 2.86 ppb decreases in  $O_3$ , while ARI induced a 1.56 ppb enhancement. The HET-driven decrease may be linked to complex nonlinear chemical responses under further reduced aerosol backgrounds, which diminished the amplification effect of radical availability. Across both phases, HET consistently emerged as the primary driver of summertime aerosol-related  $O_3$  variability. When aggregated, aerosols contributed a 1.11 ppb increase in Phase I and a 1.30 ppb decrease in Phase II, yielding a modest net summer reduction of 0.19 ppb over the CAAP period.



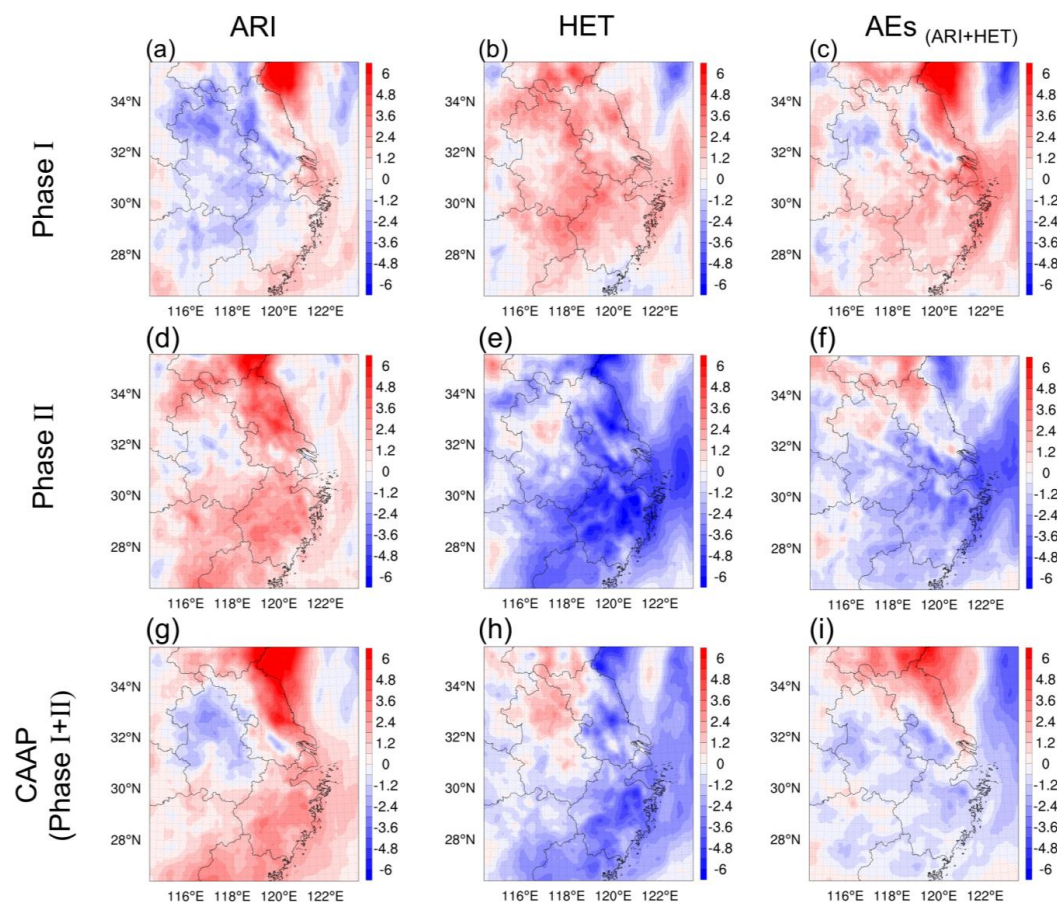


**Figure 5** Spatial distribution of summer  $O_3$  changes (ppb) over the Yangtze River Delta induced by aerosol–radiation interactions (ARI, a, d, g), heterogeneous chemistry (HET, b, e, h) and their combined effects (AEs, c, f, i) during two stages of the Clean Air Action Plan. All results are based on SET1 simulations.

To elucidate the underlying mechanisms of aerosol impacts on  $O_3$ , we examined the changes in key meteorological variables, photolysis rates, and  $HO_2$  radical concentrations induced by ARI and HET during the two implementation phases of the CAAP. Figure 6 presented the variations in five key meteorological parameters and the  $NO_2$  photolysis rate ( $J_{NO_2}$ ) in winter and summer as influenced by ARI. The results indicated that ARI consistently enhanced  $J_{NO_2}$ ,  $SW$ ,  $T_2$ ,  $WS_{10}$ , and  $PBLH$ , while reducing  $RH_2$  during winter across both phases. These modifications—especially increased  $SW$  and  $T_2$ —significantly facilitated photochemical  $O_3$  production, thereby elevating  $O_3$ . Notably, the magnitude of these changes was substantially greater in Phase I than in Phase II, which can be attributed to the more pronounced reductions in aerosol emissions during the earlier phase.

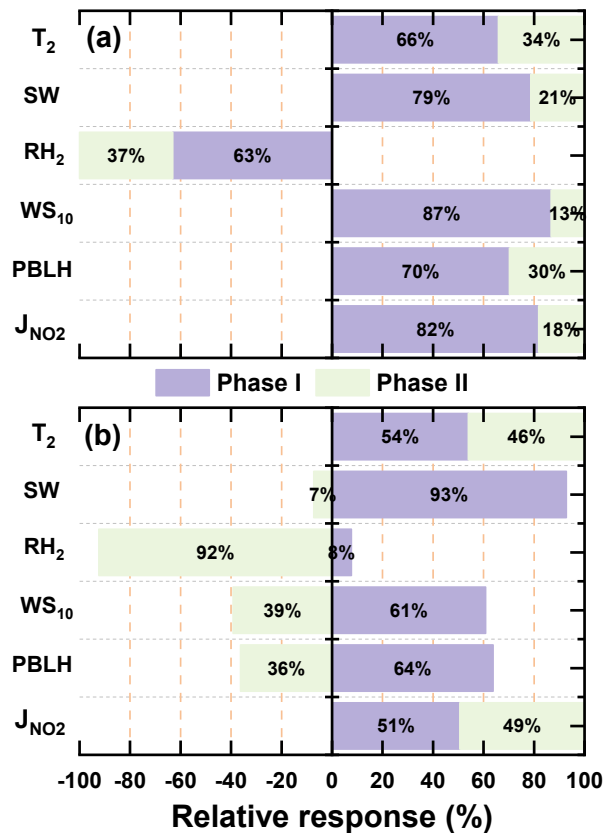


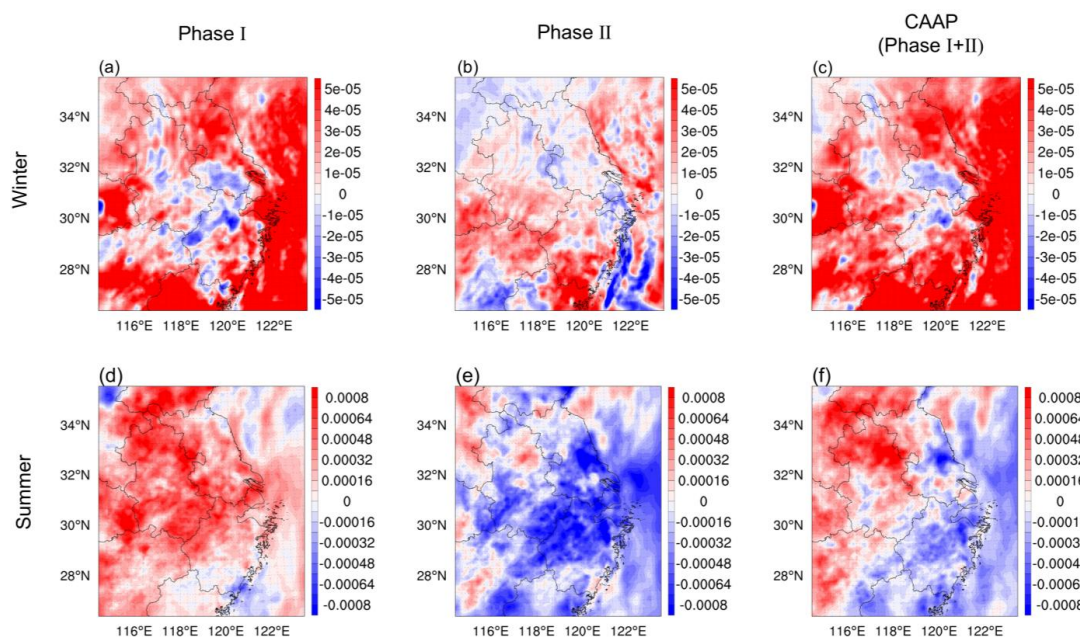
**Figure 6** Relative changes in meteorological variables and photolysis rates induced by aerosol-radiation interactions (ARI) in winter (a) and summer (b) during two phases of the Clean Air Action in the Yangtze River Delta (YRD).

In summer, ARI and HET exerted contrasting influences on ground-level  $O_3$ , with their effects reversing between the two phases. During Phase I, the substantial reduction in primary  $PM_{2.5}$  emissions (-37%) notably weakened  $HO_2$  radical uptake on aerosol surfaces, leading to elevated  $HO_2$  concentrations (Figure 7d). This increase in  $HO_2$  facilitated the conversion of NO to  $NO_2$ , thereby accelerating photochemical  $O_3$  formation. Consequently, HET contributed positively to  $O_3$  (+1.62 ppb). In contrast, ARI led to a slight decrease in  $O_3$  (-0.51 ppb), likely due to enhanced vertical mixing from reduced aerosol extinction, which increased solar radiation and photolysis rates. However, the concurrent rise in temperature and PBLH may have diluted surface  $O_3$  in certain regions (Figure 6b), resulting in a net negative  $O_3$  response to ARI during this phase. In Phase II, the magnitude of aerosol reductions was much smaller (only -8%), and drier meteorological conditions may have reduced aerosol liquid water content, thereby limiting heterogeneous interactions between  $HO_2$  radicals and aerosol surfaces. As a result, the previously positive HET effect was substantially weakened or even reversed, contributing to a net  $O_3$  reduction (-2.86 ppb). In contrast, the ARI-induced increases in  $T_2$  and photolysis rates more effectively enhanced photochemical  $O_3$  production. Simultaneously, reductions in PBLH and  $WS_{10}$  during this period suppressed vertical and horizontal  $O_3$  dispersion (Figure 6b), collectively leading to a net positive





O<sub>3</sub> response (+1.56 ppb). This phase-dependent reversal in O<sub>3</sub> responses to ARI and HET during summer underscores the nonlinear, complex, and seasonally sensitive nature of aerosol–ozone interactions. These findings highlight the necessity of jointly considering meteorological variability and aerosol physicochemical properties when assessing O<sub>3</sub> responses under evolving air quality regulations and climate change scenarios.



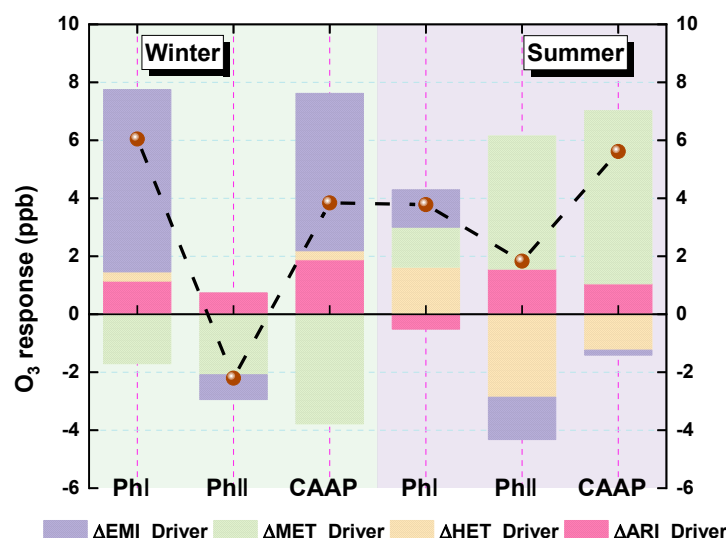
**Figure 7** Spatial distributions of HO<sub>2</sub> concentration (ppb) changes induced by aerosol heterogeneous chemistry (HET) in winter (a-c) and summer (d-f) during two phases of the Clean Air Action in the Yangtze River Delta (YRD).

Figure 8 illustrated the attribution of surface O<sub>3</sub> changes to different driving factors during the two phases of the CAAP over YRD. In winter, anthropogenic emissions emerged as the dominant driver of O<sub>3</sub> increases during Phase I, contributing 6.3 ppb, primarily due to enhanced photochemical production under VOCs-limited conditions. In contrast, Phase II saw a modest O<sub>3</sub> decline (0.9 ppb) resulting from co-reductions in NO<sub>x</sub> and VOCs, suggesting improved control effectiveness through coordinated precursor mitigation. Meteorological changes consistently exerted a suppressive effect on wintertime O<sub>3</sub>, contributing −1.7 ppb and −2.1 ppb in Phases I and II, respectively. AEs—mediated by ARI and HET—also contributed to O<sub>3</sub> accumulation, particularly in Phase I (+1.46 ppb), though their influence weakened in Phase II (+0.73 ppb) due to the smaller reductions in aerosol loading. Overall, the wintertime O<sub>3</sub> increase in Phase I was jointly driven by emissions and aerosol-related processes, while the slight decline in Phase II reflected the synergistic benefits of emission reductions and favorable meteorological conditions. In contrast, the attribution profile for summer revealed a dominant role of meteorology. Meteorological variability accounted for a substantial O<sub>3</sub> increase in Phase II (+4.6 ppb), outweighing the contributions of emission changes. The effect of emission reductions on summer O<sub>3</sub> was limited and nonlinear: a slight increase (+1.3 ppb) was observed in Phase I, followed by a minor decline (−1.5 ppb) in



Phase II, indicative of a photochemical regime with weak emission sensitivity. Aerosol-related effects exhibited strong seasonal contrasts. HET was the dominant mechanism influencing  $O_3$  in both summer phases, albeit with opposite signs—enhancing  $O_3$  by 1.62 ppb in Phase I but reducing it by 2.86 ppb in Phase II. These contrasting effects likely reflect differences in  $HO_2$  uptake efficiency under evolving humidity and temperature conditions. ARI effects were comparatively modest, leading to a slight  $O_3$  decrease in Phase I (0.51 ppb) and an increase in Phase II (1.56 ppb), likely driven by enhanced photolysis and reduced vertical mixing.

Collectively, these results highlight the evolving interplay among emission control efforts, meteorological conditions, and aerosol effects in shaping surface  $O_3$  trends. While anthropogenic emissions primarily drove winter  $O_3$  increases during the early phase of the CAAP, the roles of meteorology and aerosol processes became increasingly prominent in summer and in the later policy phase. This multi-factor attribution framework aligns well with prior modeling and observational studies in eastern China (Zhu et al., 2021; Zhou et al., 2019). For example, Liu et al. (2023) demonstrated that declining  $PM_{2.5}$  levels enhanced  $O_3$  formation by weakening  $HO_2$  radical scavenging, particularly under VOCs-limited regimes—a conclusion consistent with our wintertime results. Similarly, Yang et al. (2019) highlighted the growing influence of meteorological variability in recent years as the sensitivity of  $O_3$  to emission changes has diminished. Our study extends this knowledge base by providing phase-resolved attribution and explicitly separating the effects of ARI and HET. Notably, the reversal of HET-driven  $O_3$  responses in summer—from enhancement to suppression—has rarely been quantified and underscores the importance of dynamically characterizing aerosol–ozone interactions under evolving atmospheric and policy contexts.



**Figure 8** Attribution of surface  $O_3$  changes to different driving factors during the two phases of the Clean Air Action Plan (CAAP) over the Yangtze River Delta (YRD). Bars represent the contributions from anthropogenic emission reductions (EMI), meteorological variability (MET), aerosol–radiation interactions (ARI), and heterogeneous chemistry (HET) to winter (left) and summer (right)  $O_3$  changes during Phase I and Phase II. Units: ppb.



### 366 3.3 O<sub>3</sub> responses to precursor emission reductions under aerosol effects

367 We conducted a series of sensitivity simulations based on the 2020 emission inventory to evaluate how reductions  
368 in precursor emissions influence O<sub>3</sub> in the presence of aerosol effects. Anthropogenic emissions of five major  
369 pollutants—primary PM<sub>2.5</sub>, NO<sub>x</sub>, VOCs, NH<sub>3</sub>, and SO<sub>2</sub>—were individually reduced by 25% and 50%, while AEs  
370 (including ARI and HET) were retained. Before presenting the simulation results, we first assessed the O<sub>3</sub> chemical  
371 regimes over YRD using the widely adopted H<sub>2</sub>O<sub>2</sub>/HNO<sub>3</sub> ratio (Jeon et al., 2018; Peng et al., 2011; Hammer et al., 2002;  
372 Zhang et al., 2000). This metric serves as a diagnostic indicator of O<sub>3</sub> production sensitivity, with ratios <0.6 indicating  
373 VOCs-limited conditions, >0.8 denoting NO<sub>x</sub>-limited regimes, and intermediate values representing transitional states.  
374 Figure S5 showed the spatial distribution of this ratio under the baseline scenario (20E20M\_AEs). The analysis reveals  
375 that wintertime O<sub>3</sub> formation is predominantly VOCs-limited across the YRD, while in summer, most areas exhibit  
376 transitional or NO<sub>x</sub>-limited regimes, except parts of Anhui Province. Figure 9 displayed the simulated O<sub>3</sub> responses to  
377 precursor reductions in both seasons. The results highlight strong seasonal differences and nonlinear sensitivities  
378 depending on chemical regime. In winter, reductions in primary PM<sub>2.5</sub> and NO<sub>x</sub> led to substantial O<sub>3</sub> increases.  
379 Specifically, 25% and 50% reductions in PM<sub>2.5</sub> increased O<sub>3</sub> by 0.7 ppb and 1.5 ppb, respectively, while NO<sub>x</sub> reductions  
380 caused even larger enhancements of 4.8 ppb and 10.2 ppb. These increases primarily stem from weakened aerosol  
381 suppression mechanisms—namely reduced heterogeneous uptake and increased photolysis rates—which enhance radical  
382 availability and photochemical activity. Additionally, under VOCs-limited conditions, NO<sub>x</sub> reductions diminish O<sub>3</sub>  
383 titration by NO, further contributing to O<sub>3</sub> accumulation. Among all precursors, NO<sub>x</sub> reductions produced the most  
384 pronounced O<sub>3</sub> increase. In contrast, NH<sub>3</sub> and SO<sub>2</sub> reductions exerted negligible impacts on O<sub>3</sub>, underscoring their  
385 limited roles in direct O<sub>3</sub> photochemistry. VOCs controls, on the other hand, effectively suppressed O<sub>3</sub> formation, with  
386 25% and 50% reductions yielding decreases of 2.7 ppb and 5.6 ppb, respectively. In summer, O<sub>3</sub> responses followed  
387 broadly similar trends but with different magnitudes. Reducing PM<sub>2.5</sub> and NO<sub>x</sub> increased O<sub>3</sub> by 2 ppb and 4.3 ppb (PM<sub>2.5</sub>)  
388 and 0.8 ppb and 1.6 ppb (NO<sub>x</sub>), respectively. Notably, the O<sub>3</sub> increase associated with PM<sub>2.5</sub> reductions exceeded that  
389 from NO<sub>x</sub> cuts, underscoring the critical role of particulate matter in regulating radical chemistry via aerosol-mediated  
390 pathways. VOCs reductions remained the only control strategy that consistently decreased O<sub>3</sub>, lowering concentrations  
391 by 1.6 ppb and 3.4 ppb for 25% and 50% reductions, respectively. Again, NH<sub>3</sub> and SO<sub>2</sub> reductions had negligible effects.  
392 Collectively, these findings suggest that continued PM<sub>2.5</sub>-targeted controls may inadvertently worsen O<sub>3</sub> pollution under  
393 active AEs, particularly in summer. In contrast, VOCs mitigation remains the most robust and seasonally effective  
394 strategy for O<sub>3</sub> reduction.

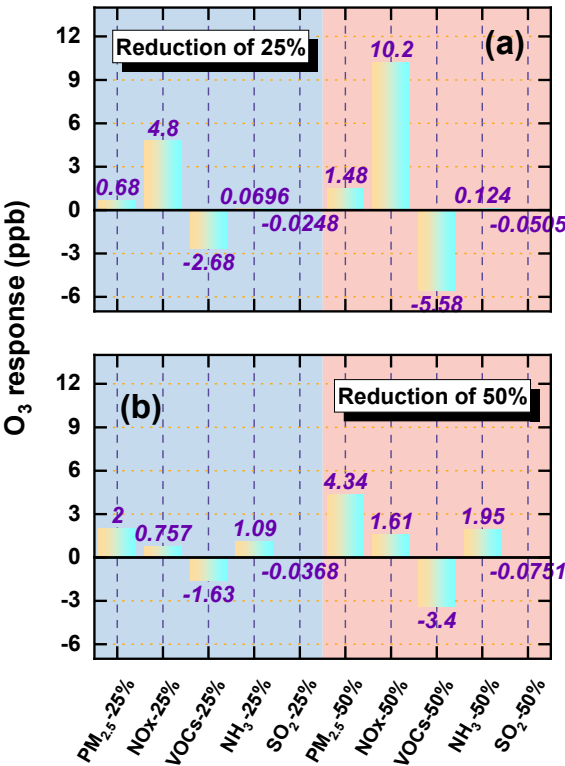


**Figure 9** O<sub>3</sub> concentration changes (ppb) in response to 25% and 50% reductions in precursor emissions over the Yangtze River Delta during winter (a) and summer (b). The columns represent different precursors: primary PM<sub>2.5</sub>, NO<sub>x</sub>, VOCs, NH<sub>3</sub>, and SO<sub>2</sub>. Simulations are based on the 2020 emission inventory and consider both aerosol–radiation interactions (ARI) and heterogeneous chemistry (HET).

Figure S6 presented the distribution of O<sub>3</sub> changes under 25% and 50% precursor reductions for both seasons. Strong seasonal contrasts and regional gradients in O<sub>3</sub> responses are evident. Reductions in PM<sub>2.5</sub> consistently caused widespread O<sub>3</sub> increases across the YRD, with the most pronounced enhancements in northwestern inland regions—particularly southern Jiangsu and central-to-northern Anhui—where historically high aerosol burdens make O<sub>3</sub> formation especially sensitive to weakened aerosol suppression (via ARI and HET). Conversely, coastal cities such as Shanghai and eastern Zhejiang exhibited smaller O<sub>3</sub> increases, reflecting their lower baseline aerosol concentrations and weaker aerosol feedbacks. VOCs reductions led to the largest O<sub>3</sub> decreases in urban corridors, particularly along the Shanghai–Nanjing–Hangzhou (SNH) axis, where VOCs emissions are elevated and O<sub>3</sub> formation is strongly VOCs-sensitive. NO<sub>x</sub> reductions yielded seasonally opposite effects: in winter, O<sub>3</sub> increased broadly across the YRD, while in summer, decreases were observed in most regions except Anhui Province. These patterns align with seasonal chemical regimes inferred from H<sub>2</sub>O<sub>2</sub>/HNO<sub>3</sub> ratios—VOCs-limited in winter and NO<sub>x</sub>-limited or transitional in summer. NH<sub>3</sub> and SO<sub>2</sub> reductions produced negligible spatial effects in both seasons, reinforcing their limited involvement in direct O<sub>3</sub> photochemistry. These spatially heterogeneous responses highlight the need for geographically differentiated control



413 strategies. Regions with historically high aerosol pollution are more likely to experience unintended O<sub>3</sub> increases  
414 following PM<sub>2.5</sub> or NO<sub>x</sub> reductions. Conversely, VOCs control provides consistent and widespread O<sub>3</sub> benefits across  
415 both seasons, making it a key lever for achieving co-benefits in both PM<sub>2.5</sub> and O<sub>3</sub> mitigation.

416 To better understand the temporal dynamics of O<sub>3</sub> responses, we analyzed diurnal variations in four representative  
417 cities—Shanghai, Nanjing, Hangzhou, and Hefei—under 50% reductions of individual precursors (Figure S7). In winter,  
418 NO<sub>x</sub> reductions led to substantial O<sub>3</sub> increases during afternoon hours (14:00–17:00), particularly in urban centers like  
419 Shanghai and Hangzhou, where enhancements exceeded 15 ppb. These increases reflect the dual effect of diminished  
420 NO titration and enhanced photochemical activity. PM<sub>2.5</sub> reductions also caused moderate O<sub>3</sub> increases from late morning  
421 to early afternoon, underscoring the influence of both ARI and HET. VOCs reductions induced midday O<sub>3</sub> declines  
422 (12:00–15:00) exceeding 5 ppb, consistent with VOCs-limited wintertime chemistry. In summer (Figure S8), VOCs  
423 reductions suppressed O<sub>3</sub> throughout the daytime, with maximum declines reaching up to 25 ppb in early afternoon,  
424 reaffirming the effectiveness of VOCs control. In contrast, PM<sub>2.5</sub> reductions led to notable O<sub>3</sub> increases during  
425 photochemically active hours (11:00–16:00), highlighting the critical role of aerosols in modulating radical cycles and  
426 O<sub>3</sub> production. Overall, these diurnal profiles underscore the time-sensitive nature of O<sub>3</sub> responses to precursor emission  
427 reductions. They emphasize the necessity for temporally and spatially refined control strategies that account for local  
428 photochemical regimes, emission structures, and AEs.

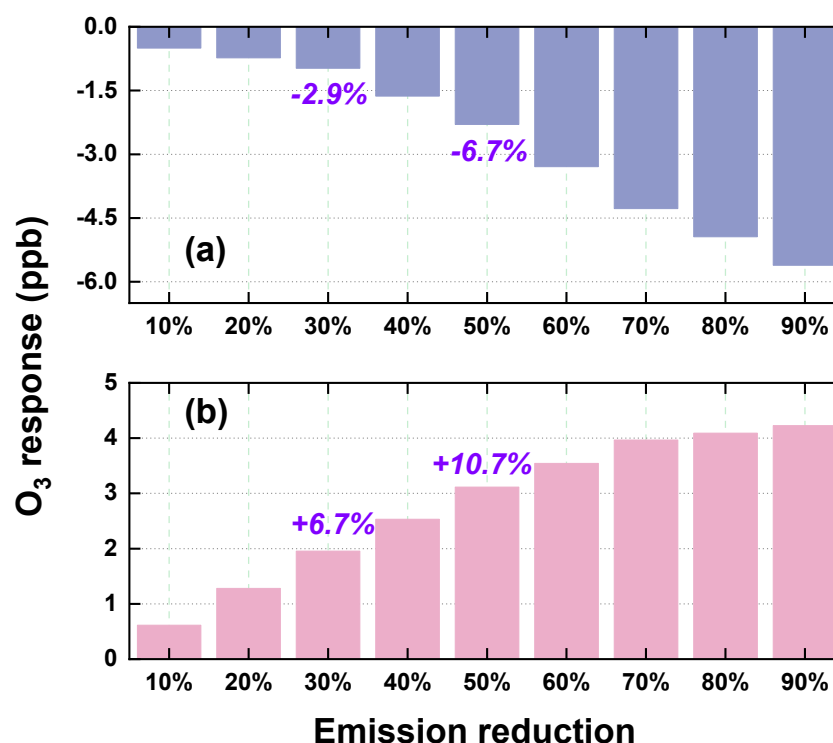
#### 429 **3.4 Future O<sub>3</sub> responses to Carbon neutrality-driven emission reductions considering aerosol effects**

430 We conducted a series of sensitivity simulations based on the 2020 anthropogenic emission inventory to assess the  
431 future responses of O<sub>3</sub> to emission reductions under China's carbon peaking and carbon neutrality strategies. Emissions  
432 were reduced by 30% and 50%, respectively, to represent projected levels during the carbon peaking and neutrality  
433 periods. These scenarios explicitly accounted for ARI and HET to more accurately capture the atmospheric responses  
434 under future air quality and climate policies. To enhance the policy relevance of our findings, additional reduction levels  
435 of 10%, 20%, 40%, 60%, 70%, 80%, and 90% were also included. As shown in Figure 10, O<sub>3</sub> exhibited pronounced  
436 seasonal variability in response to progressive emission reductions. In winter, regional mean O<sub>3</sub> increased monotonically  
437 with the magnitude of emission cuts, rising from +2.1% under the 10% reduction scenario to +14.6% under the 90%  
438 scenario. This counterintuitive increase is primarily attributed to two synergistic mechanisms: (1) reduced O<sub>3</sub> titration  
439 resulting from NO<sub>x</sub> emission reductions, and (2) weakened aerosol-mediated O<sub>3</sub> suppression due to lower aerosol loads,  
440 which diminish both ARI and HET processes. The reduced availability of aerosol surfaces and optical attenuation  
441 enhances photolysis rates and radical propagation, thereby promoting O<sub>3</sub> accumulation.

442 In contrast, summer O<sub>3</sub> declined steadily with increasing emission reductions, from -1.5% to -16.5% across the  
443 same range. This decline reflects the dominance of VOCs-limited or transitional photochemical regimes in the region



444 during summer, where coordinated reductions in NO<sub>x</sub> and VOCs effectively suppress O<sub>3</sub> formation. These results  
 445 underscore the seasonal asymmetry of O<sub>3</sub> responses under carbon neutrality-aligned emission trajectories: while  
 446 stringent reductions may inadvertently aggravate wintertime O<sub>3</sub> pollution, they offer substantial air quality co-benefits  
 447 in summer. The spatial distribution of O<sub>3</sub> changes under these scenarios, presented in Figure S9, further corroborates the  
 448 contrasting seasonal patterns. In winter, O<sub>3</sub> increases were most pronounced in inland areas of northern Anhui and central  
 449 Jiangsu—regions characterized by historically high aerosol burdens and stronger aerosol-mediated O<sub>3</sub> suppression. As  
 450 emissions decline, the weakening of both aerosol effects and NO<sub>x</sub> titration leads to a disproportionate O<sub>3</sub> rebound in  
 451 these locations. The largest summer O<sub>3</sub> reductions observed in densely populated urban corridors such as Shanghai,  
 452 Nanjing, and Hangzhou. These metropolitan areas, with high precursor emissions and transitional or NO<sub>x</sub>-limited  
 453 chemical regimes, are particularly responsive to coordinated VOCs and NO<sub>x</sub> controls. The spatial heterogeneity in O<sub>3</sub>  
 454 responses highlights the necessity of designing region-specific and seasonally adaptive emission control strategies.  
 455 Differentiated approaches are essential given the diverse pollution histories, chemical sensitivities, and aerosol–ozone  
 456 coupling characteristics across the YRD. Overall, these findings suggest that carbon neutrality–driven emission pathways,  
 457 if carefully managed, can yield significant summertime O<sub>3</sub> mitigation benefits, but must be complemented with targeted  
 458 wintertime strategies to avoid adverse trade-offs.



459 **Figure 10** Projected seasonal O<sub>3</sub> changes (ppb) under progressive emission reduction scenarios (10%-90%, 30%-carbon peak,  
 460 50%-carbon neutrality) relative to 2020 levels, incorporating aerosol effects. The upper panel shows summer responses, while  
 461 the lower panel shows winter responses.



### 463 3.5 Discussion and policy implications

464 This study presented a comprehensive assessment of O<sub>3</sub> responses to emission reductions under both the CAAP and  
465 future carbon neutrality pathways, explicitly considering aerosol effects. Our findings underscore that while emission  
466 control measures have been effective in substantially lowering PM<sub>2.5</sub>, they may yield unintended consequences for O<sub>3</sub>—  
467 pollution—particularly under VOCs-limited regimes during winter. Specifically, aerosol-induced enhancements in O<sub>3</sub>—  
468 via weakened heterogeneous chemistry (HET) and increased photolysis (ARI)—highlight the necessity of accounting  
469 for multiphase feedback mechanisms in the design of future air quality strategies.

470 Our phase-resolved, seasonally differentiated attribution analysis suggests that coordinated reductions in VOCs and  
471 NO<sub>x</sub> are critical for effective O<sub>3</sub> mitigation, especially in summer when photochemical activity is most intense.  
472 Furthermore, the spatial heterogeneity of O<sub>3</sub> responses calls for region-specific strategies. For instance, in inland areas  
473 with historically high aerosol burdens, the potential for O<sub>3</sub> rebound due to weakened aerosol suppression is more  
474 pronounced, necessitating tailored mitigation approaches. In contrast, urban corridors such as the Shanghai–Nanjing–  
475 Hangzhou (SNH) axis—characterized by high VOCs emissions and transitional or NO<sub>x</sub>-limited regimes—stand to  
476 benefit most from targeted VOCs controls, particularly under future carbon-neutrality-driven reductions.

477 It should be noted that these simulations were conducted using a fixed meteorology framework, which facilitates  
478 the isolation of aerosol and emission effects on O<sub>3</sub> by minimizing year-to-year weather variability. While this approach  
479 reduces confounding influences and enhances attribution clarity, it inherently limits the representation of  
480 meteorologically driven O<sub>3</sub> variability, such as extreme heat waves or wind anomalies. Consequently, care must be taken  
481 when extrapolating these results to long-term trends or climate-change scenarios, as meteorology-emission interactions  
482 may modulate O<sub>3</sub> responses in practice. These limitations will be addressed in our future studies through sensitivity  
483 simulations incorporating dynamic meteorology.

484 These findings carry timely relevance for China’s national climate and environmental goals. As outlined in the 14th  
485 Five-Year Plan for Ecological and Environmental Protection and the 2060 Carbon Neutrality Roadmap, deep multi-  
486 sector emission cuts are pivotal for achieving synergistic benefits between air quality improvement and climate change  
487 mitigation. Our results demonstrate that under prevailing atmospheric chemical regimes—especially during winter—  
488 aggressive reductions in primary PM<sub>2.5</sub> and NO<sub>x</sub> may inadvertently exacerbate O<sub>3</sub> pollution unless accompanied by  
489 VOCs-focused controls and regionally tailored strategies. In light of these findings, we advocate for an integrated policy  
490 framework that (i) coordinates VOCs and NO<sub>x</sub> reductions according to regional O<sub>3</sub> sensitivity, (ii) strengthens VOCs  
491 monitoring and inventory resolution at the city level, and (iii) explicitly incorporates aerosol effects in both short-term  
492 air pollution forecasting and long-term carbon-neutrality scenarios. Such targeted and mechanism-informed strategies  
493 will help bridge the current policy gap between PM<sub>2.5</sub> control and O<sub>3</sub> pollution mitigation, while ensuring co-benefits  
494 under evolving climate objectives.





#### 495 4. Conclusions

496 This study employed a phase- and season-resolved WRF-Chem modeling framework explicitly incorporating an  
497 improved aerosol–radiation interaction (ARI) scheme and a newly implemented heterogeneous chemistry (HET) module  
498 to quantify aerosol impacts on O<sub>3</sub> in the Yangtze River Delta (YRD) from 2013 to 2024. By integrating these mechanisms  
499 with anthropogenic emission changes, meteorological variability, and future carbon neutrality scenarios, we  
500 comprehensively assessed the drivers of historical and projected O<sub>3</sub> trends, as well as the nonlinear responses to precursor  
501 reductions.

502 O<sub>3</sub> exhibited a distinct rise–fall trajectory over the past decade, shaped by complex interactions among emission  
503 reductions, meteorological changes, and aerosol effects. During Phase I, substantial reductions in PM<sub>2.5</sub> and SO<sub>2</sub>, coupled  
504 with inadequate VOCs controls, led to significant wintertime O<sub>3</sub> increases (6.29 ppb) and modest summer increases (1.28  
505 ppb). In Phase II, more balanced reductions in NO<sub>x</sub> and VOCs effectively suppressed O<sub>3</sub> formation. Meteorological  
506 variability also exhibited seasonally asymmetric impacts—suppressing O<sub>3</sub> in winter but enhancing accumulation in  
507 summer. While wintertime O<sub>3</sub> changes were primarily driven by emissions, summertime variations were dominated by  
508 meteorological factors. Aerosol effects further modulated O<sub>3</sub> concentrations through seasonally distinct mechanisms. In  
509 winter, ARI played the dominant role: the substantial aerosol reductions in Phase I enhanced solar radiation and boundary  
510 layer development, promoting O<sub>3</sub> formation (1.14 ppb); these effects weakened in Phase II (0.73 ppb). In summer, HET  
511 emerged as the primary driver: in Phase I, reduced aerosols weakened radical scavenging and increased O<sub>3</sub> (1.62 ppb),  
512 whereas in Phase II, reduced HO<sub>2</sub> uptake efficiency and drier conditions reversed this effect, leading to net O<sub>3</sub> decreases  
513 (2.86 ppb).

514 Accounting for aerosol effects, precursor emission reductions elicited marked seasonal and spatial O<sub>3</sub> responses. In  
515 winter, a 50% reduction in VOCs effectively suppressed O<sub>3</sub> by 5.58 ppb, whereas equivalent reductions in NO<sub>x</sub> and  
516 PM<sub>2.5</sub> increased O<sub>3</sub> by 10.2 ppb and 1.48 ppb, respectively—primarily due to weakened O<sub>3</sub> titration and radical loss  
517 processes. In summer, reductions in PM<sub>2.5</sub> led to greater increases in O<sub>3</sub> than NO<sub>x</sub> (4.34 ppb vs. 1.61 ppb under the 50%  
518 reduction scenario), highlighting the crucial role of aerosol effects in shaping photochemical O<sub>3</sub> production. Under  
519 carbon neutrality–driven emission reduction scenarios, O<sub>3</sub> exhibited pronounced seasonally contrasting responses. In  
520 winter, O<sub>3</sub> increased monotonically with the magnitude of emission cuts, primarily due to the weakened titration by NO  
521 and the diminished aerosol-mediated suppression via heterogeneous chemistry and radiation attenuation. In contrast,  
522 summer O<sub>3</sub> consistently declined, with the most substantial improvements observed in high-emission urban corridors.  
523 These reductions were mainly driven by the synergistic control of NO<sub>x</sub> and VOCs under NO<sub>x</sub>-limited and transitional  
524 photochemical regimes. When aerosol effects were considered, wintertime O<sub>3</sub> increased by 6.7% and 10.7% under  
525 carbon peaking and neutrality scenarios, respectively, whereas summertime O<sub>3</sub> decreased by 2.9% and 6.7%,





526 highlighting the critical role of multiphase aerosol effects in shaping future air quality outcomes and making climate  
527 mitigation strategies.

528 While this study provides innovative and policy-informative findings, several uncertainties remain that warrant  
529 further investigation. Uncertainties primarily arise from limitations in the parameterization of heterogeneous chemistry,  
530 assumptions in future emission projections, and the current resolution of VOCs emission inventories. Future efforts  
531 should prioritize the enhancement of real-time VOCs monitoring, vertical profiling of O<sub>3</sub> and its precursors, and the  
532 refinement of multiphase chemical processes in regional models. In conclusion, a holistic and mechanism-informed  
533 approach—one that jointly accounts for emissions, aerosol effects, atmospheric chemistry, and meteorology—is essential  
534 for the effective co-control of PM<sub>2.5</sub> and O<sub>3</sub> in the carbon neutrality era. Seasonally adaptive, region-specific, and  
535 chemically targeted policies are critical to maximizing air quality and climate co-benefits under evolving environmental  
536 and policy contexts.

#### 537 **Code availability**

538 The WRF-Chem model (version 3.7.1) used in this study is based on the standard release from NCAR  
539 (<https://doi.org/10.5065/D6MK6B4K>), with modifications to the aerosol and chemical mechanisms. Details of these  
540 modifications are documented in Section 2.2 of the paper. The updated code about model and NCL scripts used for data  
541 processing and visualization can be provided upon request.

#### 542 **Data availability**

543 The FNL (Final Analysis) meteorological data are available from the Research Data Archive of NCAR:  
544 <http://rda.ucar.edu/datasets/ds083.2/>. The MEIC v1.4 emission inventory can be accessed at:  
545 [http://meicmodel.org/?page\\_id=560](http://meicmodel.org/?page_id=560). Hourly surface O<sub>3</sub> observations are provided by the China National Environmental  
546 Monitoring Centre (CNEMC) and are available at: <http://www.cnemc.cn/>.

#### 547 **Author contributions**

548 **YL, and TW** formulated the research, and **YL**: carried it out. **ML, YQ, HW, and MX**: technical support on the WRF-Chem  
549 model. **CL, YL, and YW**: reviewed the manuscript.

#### 550 **Competing interests**

551 The corresponding author has stated that all the authors have no conflicts of interest.

#### 552 **Disclaimer**

553 Publisher's note: Copernicus Publications remains neutral about jurisdictional claims in published maps and institutional  
554 affiliations.



555 **Financial support**

556 This investigation was supported by the National Key Basic Research & Development Program of China (2024YFC3711905),  
557 the Doctoral Scientific Research Fund of Henan Finance University (2024BS055), and the National Natural Science  
558 Foundation of China (42477103), the Creative talent exchange program for foreign experts in the Belt and Road countries, the  
559 Henan Provincial Science and Technology Research and Development Program (252102320085).



## 560 References

- 561 Cao, J., Qiu, X., Liu, Y., Yan, X., Gao, J., and Peng, L.: Identifying the dominant driver of elevated surface ozone concentration  
562 in North China plain during summertime 2012–2017, *Environ. Pollut.*, 300, 118912,  
563 <https://doi.org/10.1016/j.envpol.2022.118912>, 2022.
- 564 Chen, X., Zhong, B., Huang, F., Wang, X., Sarkar, S., Jia, S., Deng, X., Chen, D., and Shao, M.: The role of natural factors in  
565 constraining long-term tropospheric ozone trends over Southern China, *Atmos. Environ.*, 220, 117060,  
566 <https://doi.org/10.1016/j.atmosenv.2019.117060>, 2020.
- 567 Cheng, J., Tong, D., Zhang, Q., Liu, Y., Lei, Y., Yan, G., Yan, L., Yu, S., Cui, R. Y., Clarke, L., Geng, G., Zheng, B., Zhang, X.,  
568 Davis, S. J., and He, K.: Pathways of China's PM<sub>2.5</sub> air quality 2015–2060 in the context of carbon neutrality, *Natl. Sci.*  
569 *Rev.*, 8, <https://doi.org/10.1093/nsr/nwab078>, 2021.
- 570 Dai, H., Liao, H., Wang, Y., and Qian, J.: Co-occurrence of ozone and PM<sub>2.5</sub> pollution in urban/non-urban areas in eastern  
571 China from 2013 to 2020: Roles of meteorology and anthropogenic emissions, *Sci. Total Environ.*, 924, 171687,  
572 <https://doi.org/10.1016/j.scitotenv.2024.171687>, 2024.
- 573 Dai, H., Liao, H., Li, K., Yue, X., Yang, Y., Zhu, J., Jin, J., Li, B., and Jiang, X.: Composited analyses of the chemical and  
574 physical characteristics of co-polluted days by ozone and PM<sub>2.5</sub> over 2013–2020 in the Beijing–Tianjin–Hebei region,  
575 *Atmos. Chem. Phys.*, 23, 23–39, <https://doi.org/10.5194/acp-23-23-2023>, 2023.
- 576 Dang, R., Liao, H., and Fu, Y.: Quantifying the anthropogenic and meteorological influences on summertime surface ozone in  
577 China over 2012–2017, *Sci. Total Environ.*, 754, 142394, <https://doi.org/10.1016/j.scitotenv.2020.142394>, 2021.
- 578 Gao, J., Zhu, B., Xiao, H., Kang, H., Pan, C., Wang, D., and Wang, H.: Effects of black carbon and boundary layer interaction  
579 on surface ozone in Nanjing, China, *Atmos. Chem. Phys.*, 18, 7081–7094, <https://doi.org/10.5194/acp-18-7081-2018>,  
580 2018.
- 581 Geng, G., Liu, Y., Liu, Y., Liu, S., Cheng, J., Yan, L., Wu, N., Hu, H., Tong, D., and Zheng, B.: Efficacy of China's clean air  
582 actions to tackle PM<sub>2.5</sub> pollution between 2013 and 2020, *Nat. Geosci.*, 17, 987–994, [https://doi.org/10.1038/s41561-024-](https://doi.org/10.1038/s41561-024-01540-z)  
583 [01540-z](https://doi.org/10.1038/s41561-024-01540-z), 2024.
- 584 Grell, G. A., Peckham, S. E., Schmitz, R., McKeen, S. A., Frost, G., Skamarock, W. C., and Eder, B.: Fully coupled “online”  
585 chemistry within the WRF model, *Atmos. Environ.*, 39, 6957–6975, <https://doi.org/10.1016/j.atmosenv.2005.04.027>, 2005.
- 586 Guenther, A., Karl, T., Harley, P., Wiedinmyer, C., Palmer, P. I., and Geron, C.: Estimates of global terrestrial isoprene  
587 emissions using MEGAN (Model of Emissions of Gases and Aerosols from Nature), *Atmos. Chem. Phys.*, 6, 3181–3210,  
588 <https://doi.org/10.5194/acp-6-3181-2006>, 2006.
- 589 Hammer, M. U., Vogel, B., and Vogel, H.: Findings on H<sub>2</sub>O<sub>2</sub>/HNO<sub>3</sub> as an indicator of ozone sensitivity in Baden-Württemberg,  
590 Berlin-Brandenburg, and the Po valley based on numerical simulations, *J. Geophys. Res.-Atmos.*, 107, LOP 3-1-LOP 3-  
591 18, <https://doi.org/10.1029/2000JD000211>, 2002.
- 592 Hu, F., Xie, P., Xu, J., Lv, Y., Zhang, Z., Zheng, J., and Tian, X.: Long-term trends of ozone in the Yangtze River Delta, China:  
593 spatiotemporal impacts of meteorological factors, local, and non-local emissions, *J. Environ. Sci.*, 156, 408–420,  
594 <https://doi.org/10.1016/j.jes.2024.07.017>, 2025.
- 595 Jeon, W., Choi, Y., Sourì, A. H., Roy, A., Diao, L., Pan, S., Lee, H. W., and Lee, S.-H.: Identification of chemical fingerprints  
596 in long-range transport of burning induced upper tropospheric ozone from Colorado to the North Atlantic Ocean, *Sci.*  
597 *Total Environ.*, 613–614, 820–828, <https://doi.org/10.1016/j.scitotenv.2017.09.177>, 2018.
- 598 Li, K., Jacob, D. J., Liao, H., Shen, L., Zhang, Q., and Bates, K. H.: Anthropogenic drivers of 2013–2017 trends in summer  
599 surface ozone in China, *Proc. Natl. Acad. Sci.*, 116, 422–427, <https://doi.org/10.1073/pnas.1812168116>, 2019a.
- 600 Li, K., Jacob, D. J., Shen, L., Lu, X., De Smedt, I., and Liao, H.: Increases in surface ozone pollution in China from 2013 to  
601 2019: anthropogenic and meteorological influences, *Atmos. Chem. Phys.*, 20, 11423–11433, [https://doi.org/10.5194/acp-](https://doi.org/10.5194/acp-20-11423-2020)  
602 [20-11423-2020](https://doi.org/10.5194/acp-20-11423-2020), 2020.
- 603 Li, M., Wang, T., Xie, M., Li, S., Zhuang, B., Chen, P., Huang, X., and Han, Y.: Agricultural Fire Impacts on Ozone  
604 Photochemistry Over the Yangtze River Delta Region, East China, *J. Geophys. Res.-Atmos.*, 123, 6605–6623,



- 605 <https://doi.org/10.1029/2018JD028582>, 2018.
- 606 Li, M., Zhang, Q., Zheng, B., Tong, D., Lei, Y., Liu, F., Hong, C., Kang, S., Yan, L., Zhang, Y., Bo, Y., Su, H., Cheng, Y., and  
 607 He, K.: Persistent growth of anthropogenic non-methane volatile organic compound (NMVOC) emissions in China during  
 608 1990–2017: drivers, speciation and ozone formation potential, *Atmos. Chem. Phys.*, 19, 8897–8913,  
 609 <https://doi.org/10.5194/acp-19-8897-2019>, 2019b.
- 610 Li, Y., Wang, T., Wang, Q. g., Li, M., Qu, Y., Wu, H., and Xie, M.: Exploring the role of aerosol-ozone interactions on O<sub>3</sub> surge  
 611 and PM<sub>2.5</sub> decline during the clean air action period in Eastern China 2014–2020, *Atmos. Res.*, 302, 107294,  
 612 <https://doi.org/10.1016/j.atmosres.2024.107294>, 2024a.
- 613 Li, Y., Wang, T., Wang, Q. g., Li, M., Qu, Y., Wu, H., and Xie, M.: Impact of aerosol-radiation interaction and heterogeneous  
 614 chemistry on the winter decreasing PM<sub>2.5</sub> and increasing O<sub>3</sub> in Eastern China 2014–2020, *J. Environ. Sci.*, 151, 469–483,  
 615 <https://doi.org/10.1016/j.jes.2024.04.010>, 2025.
- 616 Li, Y., Wang, T., Wang, Q. g., Li, M., Qu, Y., Wu, H., Fan, J., Shao, M., and Xie, M.: Deciphering the seasonal dynamics of  
 617 multifaceted aerosol-ozone interplay: Implications for air quality management in Eastern China, *Sci. Total Environ.*, 946,  
 618 174327, <https://doi.org/10.1016/j.scitotenv.2024.174327>, 2024b.
- 619 Li, Y., Wang, T., Wang, Q. g., Qu, Y., Wu, H., Xie, M., Li, M., Li, S., and Zhuang, B.: Spatiotemporal Variations of PM<sub>2.5</sub> and  
 620 O<sub>3</sub> Relationship during 2014–2021 in Eastern China, *Aerosol. Air. Qual. Res.*, 23, 230060,  
 621 <https://doi.org/10.4209/aaqr.230060>, 2023.
- 622 Liu, H., Liu, S., Xue, B., Lv, Z., Meng, Z., Yang, X., Xue, T., Yu, Q., and He, K.: Ground-level ozone pollution and its health  
 623 impacts in China, *Atmos. Environ.*, 173, 223–230, <https://doi.org/10.1016/j.atmosenv.2017.11.014>, 2018.
- 624 Liu, Y. and Wang, T.: Worsening urban ozone pollution in China from 2013 to 2017 – Part 1: The complex and varying roles  
 625 of meteorology, *Atmos. Chem. Phys.*, 20, 6305–6321, <https://doi.org/10.5194/acp-20-6305-2020>, 2020.
- 626 Liu, Y., Geng, G., Cheng, J., Liu, Y., Xiao, Q., Liu, L., Shi, Q., Tong, D., He, K., and Zhang, Q.: Drivers of Increasing Ozone  
 627 during the Two Phases of Clean Air Actions in China 2013–2020, *Environ. Sci. Technol.*, 57, 8954–8964,  
 628 <https://doi.org/10.1021/acs.est.3c00054>, 2023.
- 629 Lu, S., Gong, S., Chen, J., Zhang, L., Ke, H., Pan, W., Lu, J., and You, Y.: Contribution assessment of meteorology vs. emissions  
 630 in the summer ozone trend from 2014 to 2023 in China by an environmental meteorology index, *Atmos. Environ.*, 343,  
 631 120992, <https://doi.org/10.1016/j.atmosenv.2024.120992>, 2025.
- 632 Ma, D., Wang, T., Wu, H., Qu, Y., Liu, J., Liu, J., Li, S., Zhuang, B., Li, M., and Xie, M.: The effect of anthropogenic emission,  
 633 meteorological factors, and carbon dioxide on the surface ozone increase in China from 2008 to 2018 during the East  
 634 Asia summer monsoon season, *Atmos. Chem. Phys.*, 23, 6525–6544, <https://doi.org/10.5194/acp-23-6525-2023>, 2023.
- 635 Ni, Y., Yang, Y., Wang, H., Li, H., Li, M., Wang, P., Li, K., and Liao, H.: Contrasting changes in ozone during 2019–2021  
 636 between eastern and the other regions of China attributed to anthropogenic emissions and meteorological conditions, *Sci.*  
 637 *Total Environ.*, 908, 168272, <https://doi.org/10.1016/j.scitotenv.2023.168272>, 2024.
- 638 Peng, Y.-P., Chen, K.-S., Wang, H.-K., Lai, C.-H., Lin, M.-H., and Lee, C.-H.: Applying model simulation and photochemical  
 639 indicators to evaluate ozone sensitivity in southern Taiwan, *J. Environ. Sci.*, 23, 790–797, [https://doi.org/10.1016/S1001-0742\(10\)60479-2](https://doi.org/10.1016/S1001-0742(10)60479-2), 2011.
- 640
- 641 Qu, Y., Wang, T., Yuan, C., Wu, H., Gao, L., Huang, C., Li, Y., Li, M., and Xie, M.: The underlying mechanisms of PM<sub>2.5</sub> and  
 642 O<sub>3</sub> synergistic pollution in East China: Photochemical and heterogeneous interactions, *Sci. Total Environ.*, 873, 162434,  
 643 <https://doi.org/10.1016/j.scitotenv.2023.162434>, 2023.
- 644 Shao, M., Lv, S., Song, Y., Liu, R., and Dai, Q.: Disentangling the effects of meteorology and emissions from anthropogenic  
 645 and biogenic sources on the increased surface ozone in Eastern China, *Atmos. Res.*, 311, 107699,  
 646 <https://doi.org/10.1016/j.atmosres.2024.107699>, 2024.
- 647 Sun, L., Xue, L., Wang, Y., Li, L., Lin, J., Ni, R., Yan, Y., Chen, L., Li, J., and Zhang, Q.: Impacts of meteorology and emissions  
 648 on summertime surface ozone increases over central eastern China between 2003 and 2015, *Atmos. Chem. Phys.*, 19,  
 649 1455–1469, <https://doi.org/10.5194/acp-19-1455-2019>, 2019.
- 650 Wu, K., Wang, Y., Qiao, Y., Liu, Y., Wang, S., Yang, X., Wang, H., Lu, Y., Zhang, X., and Lei, Y.: Drivers of 2013–2020 ozone  
 651 trends in the Sichuan Basin, China: Impacts of meteorology and precursor emission changes, *Environ. Pollut.*, 300,



- 118914, <https://doi.org/10.1016/j.envpol.2022.118914>, 2022.
- Yan, D., Jin, Z., Zhou, Y., Li, M., Zhang, Z., Wang, T., Zhuang, B., Li, S., and Xie, M.: Anthropogenically and meteorologically modulated summertime ozone trends and their health implications since China's clean air actions, *Environ. Pollut.*, 343, 123234, <https://doi.org/10.1016/j.envpol.2023.123234>, 2024.
- Yang, H., Chen, L., Liao, H., Zhu, J., Wang, W., and Li, X.: Weakened aerosol–radiation interaction exacerbating ozone pollution in eastern China since China's clean air actions, *Atmos. Chem. Phys.*, 24, 4001–4015, <https://doi.org/10.5194/acp-24-4001-2024>, 2024.
- Yang, L., Luo, H., Yuan, Z., Zheng, J., Huang, Z., Li, C., Lin, X., Louie, P. K. K., Chen, D., and Bian, Y.: Quantitative impacts of meteorology and precursor emission changes on the long-term trend of ambient ozone over the Pearl River Delta, China, and implications for ozone control strategy, *Atmos. Chem. Phys.*, 19, 12901–12916, <https://doi.org/10.5194/acp-19-12901-2019>, 2019.
- Yin, H., Lu, X., Sun, Y., Li, K., Gao, M., Zheng, B., and Liu, C.: Unprecedented decline in summertime surface ozone over eastern China in 2020 comparably attributable to anthropogenic emission reductions and meteorology, *Environ. Res. Lett.*, 16, 124069, <https://doi.org/10.1088/1748-9326/ac3e22>, 2021.
- Yu, Y., Wang, Z., He, T., Meng, X., Xie, S., and Yu, H.: Driving factors of the significant increase in surface ozone in the Yangtze River Delta, China, during 2013–2017, *Atmos. Pollut. Res.*, 10, 1357–1364, <https://doi.org/10.1016/j.apr.2019.03.010>, 2019.
- Zhai, S., Jacob, D. J., Wang, X., Shen, L., Li, K., Zhang, Y., Gui, K., Zhao, T., and Liao, H.: Fine particulate matter (PM<sub>2.5</sub>) trends in China, 2013–2018: Separating contributions from anthropogenic emissions and meteorology, *Atmos. Chem. Phys.*, 19, 11031–11041, <https://doi.org/10.5194/acp-19-11031-2019>, 2019.
- Zhang, H., Roehl, C. M., Sander, S. P., and Wennberg, P. O.: Intensity of the second and third OH overtones of H<sub>2</sub>O<sub>2</sub>, HNO<sub>3</sub>, and HO<sub>2</sub>NO<sub>2</sub>, *J. Geophys. Res.-Atmos.*, 105, 14593–14598, <https://doi.org/10.1029/2000JD900118>, 2000.
- Zhang, X., Zhang, W.-C., Wu, W., and Liu, H.-B.: Understanding ozone variability in spatial responses to emissions and meteorology in China using interpretable machine learning, *iScience.*, 28, 113036, <https://doi.org/10.1016/j.isci.2025.113036>, 2025.
- Zhao, X., Zhang, Z., Xu, J., Gao, J., Cheng, S., Zhao, X., Xia, X., and Hu, B.: Impacts of aerosol direct effects on PM<sub>2.5</sub> and O<sub>3</sub> respond to the reductions of different primary emissions in Beijing-Tianjin-Hebei and surrounding area, *Atmos. Environ.*, 309, 119948, <https://doi.org/10.1016/j.atmosenv.2023.119948>, 2023.
- Zhou, M., Zhang, L., Chen, D., Gu, Y., Fu, T.-M., Gao, M., Zhao, Y., Lu, X., and Zhao, B.: The impact of aerosol–radiation interactions on the effectiveness of emission control measures, *Environ. Res. Lett.*, 14, 024002, <https://doi.org/10.1088/1748-9326/aaf27d>, 2019.
- Zhu, J., Chen, L., Liao, H., Yang, H., Yang, Y., and Yue, X.: Enhanced PM<sub>2.5</sub> Decreases and O<sub>3</sub> Increases in China During COVID-19 Lockdown by Aerosol-Radiation Feedback, *Geophys. Res. Lett.*, 48, e2020GL090260, <https://doi.org/10.1029/2020GL090260>, 2021.